Determination of Gas-Phase Ligand Binding Energies to Mg^+ by FTMS Techniques

Lorenza Operti,[1] Edward C. Tews, and Ben S. Freiser*

Contribution from the Chemistry Department, Purdue University, West Lafayette, Indiana 47907. *Received July 20, 1987*

Abstract: Relative and absolute gas-phase binding energies of 12 organic molecules to Mg^+ have been determined by four different methods involving Fourier transform mass spectrometry (FTMS). Mg^+ is generated in the FTMS cell by pulsed laser ionization and reacts with the organic compounds to give MgL^+ either by direct condensation or by a fast two-step displacement reaction. The equilibrium constant (K_{eq}) and the absolute rate constants (k_f and k_r) are obtained for the ligand exchange reaction: $MgL^+ + L' \rightleftharpoons MgL'^+ + L$. The equilibrium constants are converted to free-energy differences and relative binding energies are calculated to give the $D°(Mg^+–L)$ scale. Entropy changes are assumed to be small and they are discussed in detail. The absolute gas-phase binding energies $D°(Mg^+–MeOH)$ and $D°(Mg^+–Me_2CO)$ are assigned from equilibrium and photodissociation experiments to be 61 ± 5 and 67 ± 5 kcal/mol, respectively. The correlation of results from the different methods give a scale of relative and absolute bond energies to Mg^+ for the 12 organic molecules examined. The results for Mg^+ are compared with previously reported results on H^+, $CpNi^+$, Al^+, Mn^+, and Cu^+. These comparisons show for this limited study on oxygen bases that Mg^+ is a softer acid than H^+ and Al^+, very similar in acidity to Mn^+ and Cu^+, and a harder acid than $CpNi^+$.

Over the past few years, the study of gas-phase organometallic ion chemistry has experienced a rapid growth. A wide variety of mass spectrometric techniques has been brought to bear on the problem, yielding a wealth of fundamental thermochemical, kinetic, and mechanistic information.[2-5] In particular, the determination of gas-phase binding energies of organic molecules to metal cations, which is the enthalpy of reaction 1, has provided

$$ML^+ \rightarrow M^+ + L \qquad \Delta H = D°(M^+–L) \qquad (1)$$

important thermochemical data useful in evaluating the energetics of catalytic processes and the feasibility of proposed reaction pathways.

In obtaining metal ion–ligand bond energies, it is desirable to use a variety of complementary methods as a cross-check of the results. One of the most powerful tools for determining absolute metal ion–ligand binding energies is the ion beam instrument which is used to obtain accurate thresholds for endothermic reactions.[6] Ion cyclotron resonance (ICR) spectroscopy has been applied extensively to measure relative ligand binding energies from equilibrium ligand-exchange reactions.[7,8] Limits on these energies can be obtained from observation of exothermic ion–molecule reactions. More recently, photodissociation experiments have shown promise for yielding absolute metal ion–ligand binding energies.[9,10]

In this paper we report the determination of the gas-phase ligand binding energies to Mg^+ for a series of alcohols, aldehydes, ethers, and ketones. Interest in the gaseous chemistry of magnesium is derived in part from its role in ionospheric processes.[11] In this regard we have recently completed a study on the thermochemical properties of MgO^+ and $MgOH^+$.[12] Moreover, Mg^+ is of interest because it provides an additional comparison of the behavior of a metallic species having no d electrons, such as Al^+.[7a]

Four different techniques involving Fourier transform mass spectrometry (FTMS) have been used in this research: collision-induced dissociation (CID), photodissociation, and the determination of equilibrium constants by both steady-state and kinetic methods. The data obtained by steady-state equilibrium and kinetic measurements are compared quantitatively, and in turn both are compared qualitatively to the relative bond ordering obtained by collision-induced dissociation experiments. Finally, photodissociation experiments can provide absolute bond energies, $D°(Mg^+–L)$, and permit another cross-check of the different methods. The dependence of $D°(Mg^+–L)$ on functional group is analyzed, as well as the observed substituent effects. The results of Mg^+ are compared with results obtained previously for other cations: H^+,[13] $CpNi^+$,[14] Al^+,[7a] Mn^+,[7b] and Cu^+.[7c]

Experimental Section

The theory, instrumentation, and methodology of Fourier transform mass spectrometry (FTMS) have been discussed elsewhere.[15] CID experiments, as well as equilibrium and absolute rate constant determinations, were performed on a Nicolet FTMS-2000 Fourier transform mass spectrometer. The instrument is equipped with a differentially pumped dual analysis cell (source side and analyzer side), which is situated in the bore of a superconducting magnet maintained at 3 T. The two 4.8-cm cubic cells share one common side, referred to as the conductance limit, which consists of a solid plate with a 2-mm diameter orifice. For this study, however, the system was operated as a single cell

(1) On leave from Istituto di Chimica Generale ed Inorganica, Universita' di Torino, Italy.

(2) (a) Armentrout, P. B.; Loh, S. K.; Ervin, K. M. *J. Am. Chem. Soc.* **1984**, *106*, 1161. (b) Houriet, R.; Halle, L. F.; Beauchamp, J. L. *Organometallics* **1982**, *2*, 1818.

(3) (a) Allison, J.; Radecki, B. *J. Am. Chem. Soc.* **1984**, *106*, 946. (b) Larsen, B. S.; Ridge, D. P. *Ibid.* **1984**, *106*, 1912. (c) Allison, J. *Prog. Inorg. Chem.* **1986**, *34*, 627.

(4) (a) Jacobson, D. B.; Freiser, B. S. *J. Am. Chem. Soc.* **1985**, *107*, 1581. (b) Morse, M. D.; Smalley, R. E. *Ber. Bunsenges. Phys. Chem.* **1984**, *88*, 228. (c) Anderson-Fredeen, D. J.; Russell, D. H. *J. Am. Chem. Soc.* **1985**, *107*, 3762.

(5) (a) Lane, K. R.; Sallans, L.; Squires, R. R. *Organometallics* **1985**, *4*, 408. (b) Tonkyn, R.; Weisshaar, J. C. *J. Phys. Chem.* **1986**, *90*, 2305.

(6) (a) Armentrout, P. B.; Halle, L. F.; Beauchamp, J. L. *J. Am. Chem. Soc.* **1981**, *103*, 6501. (b) Armentrout, P. B.; Beauchamp, J. L. *J. Chem. Phys.* **1981**, *74*, 2819.

(7) (a) Uppal, J. S.; Staley, R. H. *J. Am. Chem. Soc.* **1982**, *104*, 1235. (b) Uppal, J. S.; Staley, R. H. *Ibid.* **1982**, *104*, 1238. (c) Jones, R. W.; Staley, R. H. *Ibid.* **1982**, *104*, 2296.

(8) (a) Cody, R. B.; Burnier, R. C.; Reents, W. D., Jr.; Carlin, T. J.; McCrery, D. H.; Lengel, R. K.; Freiser, B. S. *Int. J. Mass Spectrom. Ion Phys.* **1980**, *33*, 37. (b) Burnier, R. C.; Carlin, T. J.; Reents, W. D., Jr.; Cody, R. B.; Lengel, R. K.; Freiser, B. S. *J. Am. Chem. Soc.* **1979**, *101*, 7127.

(9) Dunbar, R. C. In *Gas Phase Ion Chemistry*; Bowers, M. T., Ed.; Academic Press: New York, 1984; Vol. 3, Chapter 20.

(10) (a) Hettich, R. L.; Freiser, B. S. *J. Am. Chem. Soc.* **1986**, *108*, 2537. (b) Hettich, R. L.; Jackson, T. C.; Stanko, E. M.; Freiser, B. S. *Ibid.* **1986**, *108*, 5086.

(11) (a) Murad, E.; Swider, W.; Benson, S. W. *Nature (London)* **1981**, *289*, 273. (b) Murad, E. *J. Chem. Phys.* **1981**, *75*, 4080.

(12) Operti, L.; Tews, E. C.; Freiser, B. S. *J. Phys. Chem.*, to be submitted for publication.

(13) Aue, D. H.; Bowers, M. T. In *Gas Phase Ion Chemistry*; Bowers, M. T., Ed.; Academic Press: New York, 1979; Vol. 2, Chapter 9.

(14) Corderman, R. R.; Beauchamp, J. L. *J. Am. Chem. Soc.* **1976**, *98*, 3998.

(15) (a) Comisarow, M. B. *Adv. Mass Spectrom.* **1980**, *8*, 1698. (b) Gross, M. L.; Rempel, D. L. *Science* **1984**, *226*, 261. (c) Marshall, A. G. *Acc. Chem. Res.* **1985**, *18*, 316. (d) Freiser, B. S. *Talanta* **1985**, *32*, 697. (e) Laude, D. A., Jr.; Johlman, C. L.; Brown, R. S.; Weil, D. A.; Wilkins, C. L. *Mass Spectrom. Rev.* **1986**, *5*, 107.

0002-7863/88/1510-3847$01.50/0

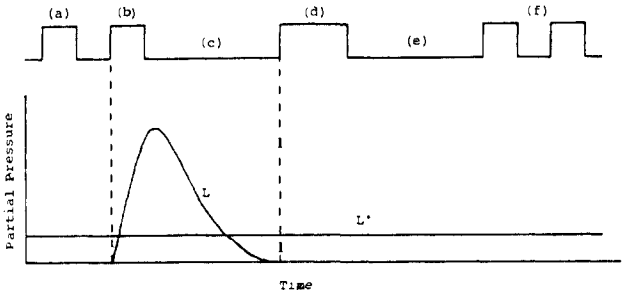

Figure 1. Experimental sequence for the determination of the absolute rate constant of reaction 3: (a) quench; (b) laser desorb Mg^+ ions; (c) reaction of Mg^+ with L and L′, both present in the cell, to generate MgL^+, MgL'^+, and other ions; (d) isolation of MgL^+ ion, L has been pumped away; (e) MgL^+ reacts with L′ to form MgL'^+; (f) excitation and detection.

instrument with all of the experiments performed in the source cell side. Mg^+ was generated by focusing the beam (1064 nm) of a pulsed Quanta Ray Nd–YAG laser onto a magnesium target which was mounted on the solids probe tip. The internal optics used to direct the laser beam were those which come standard with the FTMS-2000.

Chemicals were obtained commercially in high purity and were used as supplied except for multiple freeze–pump–thaw cycles to remove noncondensable gases. The samples were admitted to the cell through a modified inlet system using either a Varian leak valve or a General Valve Corp. Series 9 pulsed solenoid valve.[16] The pulsed gas profile was approximately 1 s wide and reached a maximum of $\sim 10^{-5}$ torr at about 400 ms. A Bayard-Alpert ionization gauge was used to measure static pressures. The gauge was calibrated to ethane by monitoring the rate of reaction 2 and correlating the result to the reported rate constant, k

$$C_2H_5^+ + C_2H_6 \rightarrow C_4H_9^+ + H_2 \qquad (2)$$

$= 4.0 \times 10^{-11} \pm 0.4$ cm^3 molecule^{-1} s^{-1}.[17] The calculated correction coefficients for other gases with respect to ethane were then applied to estimate pressures.[18] Argon was used as the collision gas for CID at a total pressure of about 5×10^{-6} torr. Details of the CID experiment have previously been discussed.[19] Binary gas mixtures were prepared in the cell by admitting the gases through two different leak valves. Partial pressures were determined as the difference between the total pressure and background for the first reagent and between the new total pressure and previous total pressure for the second one. A delay of a couple of minutes was generally required in order to obtain stable pressure readings. The reversed procedure was repeated at the end of each experiment by closing one leak valve at a time.

Binary gas mixtures of the compounds, L and L′, were used to measure the equilibrium constant of ligand-exchange reaction 3. Absolute

$$MgL^+ + L' \underset{k_r}{\overset{k_f}{\rightleftharpoons}} MgL'^+ + L \qquad (3)$$

rate constant determinations of k_f and k_r for reaction 3 were performed by introducing L through a pulsed valve and L′ through a leak valve in the cell. Mg^+, generated by laser desorption, was allowed to react with both compounds, L and L′, forming primarily MgL^+ and MgL'^+. After L has been pumped away, MgL^+ was isolated by double resonance pulses.[20] Next, the time of the reaction of MgL^+ with L′ was varied yielding ligand substitution to form MgL'^+. The intensities of MgL^+ and MgL'^+ were monitored versus time to give absolute rate constants. A typical timing sequence and pressure profile for these experiments are shown in Figure 1.

Formation of MgL^+ by direct association of Mg^+ with a ligand L is highly exothermic and, therefore, must initially result in MgL^+ being internally excited. Observation of MgL^+ formed under bimolecular conditions, however, indicates that IR radiative relaxation can compete with unimolecular dissociation of MgL^+ back to Mg^+ and L. Collisional cooling is effective in removing the majority of the remaining internal energy as evidenced by the single exponential behavior observed in measuring k_f and k_r and by the excellent agreement between the measurement of K_{eq} and k_f/k_r. However, the presence of a small population of excited ions cannot be completely ruled out. In the photodissociation threshold experiments, any excess internal energies present in the ion could lead to an estimate of the bond energy which is too low.

Table I. Experimental and Calculated Rate Constants[a] for Condensation Reaction 4

ligand (L)	k(exptl)[b]	k(ADO)[c]	% efficiency[d]
MeOH	7.0×10^{-12}	2.03×10^{-9}	0.34
EtOH	1.5×10^{-11}	2.07×10^{-9}	0.72
n-PrOH	1.4×10^{-10}	2.07×10^{-9}	6.8
i-PrOH[e]	1.1×10^{-9}	2.13×10^{-9}	52
n-BuOH	7.0×10^{-10}	2.17×10^{-9}	32
MeCHO	6.1×10^{-11}	2.78×10^{-9}	2.2
EtCHO	9.2×10^{-11}	2.67×10^{-9}	3.4
n-PrCHO	8.5×10^{-10}	2.82×10^{-9}	30

[a] Rate constants are expressed in cm^3 molecule^{-1} s^{-1}. [b] Experimental rate constants are obtained at pressures of L in the range $2–5 \times 10^{-7}$ torr. [c] Calculated according to ADO theory, ref 23, using dipole moments from ref 24 and polarizabilities from ref 25. [d] Efficiency = (k(exptl)/k(ADO)) × 100. [e] Rate constant of reaction 5.

Photodissocation experiments were performed on a Nicolet prototype FTMS-1000 Fourier transform mass spectrometer previously described in detail.[21] This instrument is equipped with a 5.2-cm cubic trapping cell situated between the poles of a Varian 15-in. electromagnet maintained at 0.9 T. The cell, constructed in our laboratory, utilizes two 80% transmittance stainless steel screens as the transmitter plates. This arrangement permits irradiation with a 2.5-kW Hg–Xe arc lamp, used in conjunction with a set of cutoff filters. Mg^+ was generated by focusing the beam of a Quanta Ray Nd–YAG pulsed laser (1064 nm) into the center-drilled hole (1 mm) of a magnesium rod supported on the transmittance screen nearest to the laser.

All samples were admitted to the cell through a General Valve Corp. Series 9 pulsed solenoid valve,[22] which was triggered concurrently with the laser pulse. The pulsed sample pressure had a rise time of about 200 ms, reached a maximum pressure of approximately 10^{-5} torr, and was pumped away by a high-speed diffusion pump in about 400 ms. Isolation of the ion of interest by swept double resonance pulses[20] allowed the ion to be trapped for periods of 10–15 s in either the presence or absence of light.

Photodissociation was monitored by the appearance of ionic photoproducts as a function of light transmitted by the cutoff filters. Energies corresponding to 1% transmittance were assigned to each cutoff filter. Because of laser shot-to-shot variation, appearances of the photoproducts were monitored and normalized as intensity(photoproduct)/intensity(parent). The threshold was bracketed between the lowest energy at which photodissociation products were observed and the highest energy at which they were not distinguishable from the blank. Details of photodissociation experiments have been described elsewhere.[10b]

Results

Each of the organic compounds studied reacts with Mg^+ to form MgL^+ (L = compound) by direct condensation, reaction 4, with

$$Mg^+ + L \rightarrow MgL^+ \qquad (4)$$

the exception of the branched C_3–C_4 alcohols which generate MgL^+ by a two-step sequence, reactions 5 and 6, involving a

$$Mg^+ + ROH \rightarrow Mg(H_2O)^+ + \text{alkene} \qquad (5)$$

$$Mg(H_2O)^+ + ROH \rightarrow Mg(ROH)^+ + H_2O \qquad (6)$$

$Mg(H_2O)^+$ intermediate.

With regard to organic ligands of the same class (alcohols, aldehydes, ethers, or ketones), the rate of disappearance of Mg^+ increases with increasing size of the alkyl substituent of the functional group as expected. For example, the rate constants for Mg^+ with MeOH, EtOH, *n*-PrOH, and *n*-BuOH by reaction 4 are 7.0×10^{-12}, 1.5×10^{-11}, 1.4×10^{-10}, and 7.0×10^{-10} cm^3 molecule^{-1} s^{-1}, respectively. For comparison, a rate constant of 1.1×10^{-9} cm^3 molecule^{-1} s^{-1} is observed for Mg^+ reacting with *i*-PrOH by reaction 5. The rate constants for the condensation reaction 4 of aldehydes are 6.1×10^{-11}, 9.2×10^{-11}, and 8.5×10^{-10} cm^3 molecule^{-1} s^{-1} for MeCHO, EtCHO, and *n*-PrCHO,

(16) Tews, E. C. Ph.D. Thesis, Purdue University, 1987.
(17) Kim, J. K.; Anicich, V. G.; Huntress, W. T. *J. Phys. Chem.* **1977**, *81*, 1978.
(18) Bartmess, J. E.; Georgiadis, R. M. *Vacuum* **1983**, *33*, 149.
(19) (a) Jacobson, D. B.; Freiser, B. S. *J. Am. Chem. Soc.* **1983**, *105*, 736. (b) Jacobson, D. B.; Freiser, B. S. *Ibid.* **1983**, *105*, 7484.
(20) Comisarow, M. B.; Parisod, G.; Grassi, V. *Chem. Phys. Lett.* **1978**, *57*, 413.
(21) Cody, R. B.; Burnier, R. C.; Freiser, B. S. *Anal. Chem.* **1982**, *54*, 96.
(22) Carlin, T. J.; Freiser, B. S. *Anal. Chem.* **1983**, *55*, 571.

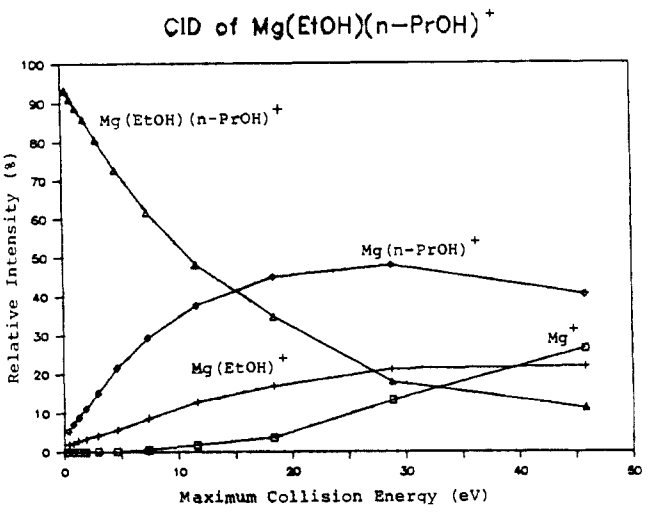

Figure 2. Variation of ion abundances with increasing kinetic energy (laboratory frame) from CID of the parent $Mg(EtOH)(n\text{-}PrOH)^+$.

respectively. Table I compares these rate constants together with those obtained from ADO calculations. Rate constants for the reaction of Mg^+ with *n*-PrOH (reaction 4) and *i*-PrOH (reaction 5) have previously been determined by ICR techniques.[26] However, the reported values of 7×10^{-10} and 6×10^{-10} cm^3 $molecule^{-1}$ s^{-1} for *n*-PrOH and *i*-PrOH, respectively, disagree significantly with this study. In addition, the earlier work indicated no reaction occurs between Mg^+ and methanol or ethanol. One possible explanation for this discrepancy is the decreased sensitivity of ICR compared to FTMS.

A second condensation reaction at a slower rate is usually observed, reaction 7, leading to $Mg(L)_2^+$ as the final product. A

$$MgL^+ + L \rightarrow Mg(L)_2^+ \qquad (7)$$

rate constant $k = 1.2 \times 10^{-10}$ cm^3 $molecule^{-1}$ s^{-1} has been measured for L = *n*-BuOH. A slower rate of condensation of a second ligand is somewhat surprising in view of the greater number of vibrational modes afforded by the additional ligand. Steric effects or, more likely, a reduction in the bond energy of the second ligand may explain these results.

In the presence of binary mixtures of ligand molecules, L and L′, displacement reactions take place for both the MgL^+, reaction 3, and the $Mg(L)_2^+$ species, reactions 8 and 9. A low total

$$Mg(L)_2^+ + L' \rightleftharpoons MgLL'^+ + L \qquad (8)$$

$$MgLL'^+ + L' \rightleftharpoons Mg(L')_2^+ + L \qquad (9)$$

pressure ($\sim 5.0 \times 10^{-7}$ torr) is generally required in order to minimize $Mg(L)_2^+$ formation. In this way ligand exchange, reaction 3, can reach equilibrium before secondary condensation, reaction 7, becomes important.

Collision-induced dissociation (CID) experiments on $MgLL'^+$ ions were usually performed before equilibrium and kinetic measurements in order to provide qualitative information on the relative bond strengths of L and L′ to Mg^+.[19,27] CID results, indicating which ligand is more strongly bound to Mg^+ and allowing an estimate of the magnitude of the difference, are useful for the choice of experimental conditions for the equilibrium experiments such as L/L′ relative partial pressures. Moreover, they provide a cross-check of data obtained by the other methods. Figure 2 shows the variation of ion abundances with increasing kinetic energy from the CID of $Mg(EtOH)(n\text{-}PrOH)^+$. At low energies the abundance of $Mg(n\text{-}PrOH)^+$ is greater and increases faster than that of $Mg(EtOH)^+$. At higher energies, Mg^+ also appears. This behavior suggests that $D(Mg^+\text{–}n\text{-}PrOH) > D(Mg^+\text{–}EtOH)$.

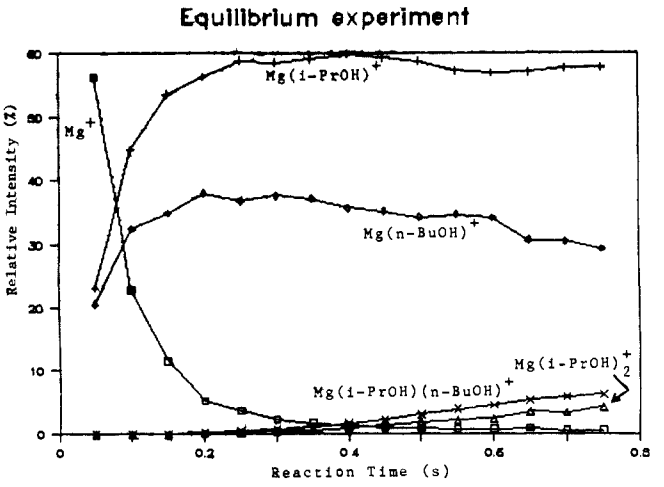

Figure 3. Variation of ion abundances with time for Mg^+ with a 3:1 mixture of *i*-PrOH and *n*-BuOH, at a total pressure of 5×10^{-7} torr.

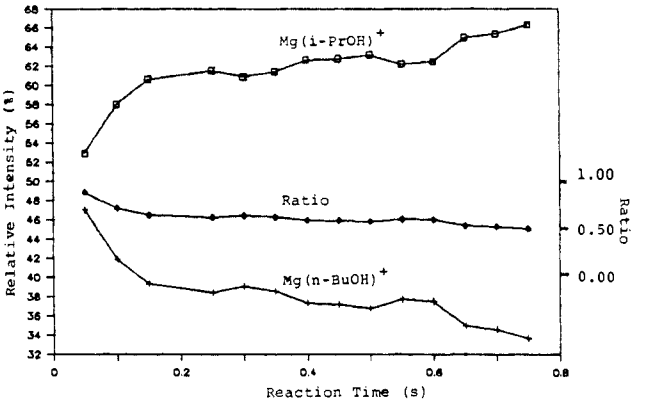

Figure 4. Relative abundances of $Mg(n\text{-}BuOH)^+$ and $Mg(i\text{-}PrOH)^+$ and their ratio $Mg(n\text{-}BuOH)^+/Mg(i\text{-}PrOH)^+$ as a function of time for the same reacting system as in Figure 3.

Figure 3 shows the variation of ion abundance with time for a 3:1 mixture of *i*-PrOH and *n*-BuOH. Following initial reaction, the ratio of $Mg(i\text{-}PrOH)^+$ and $Mg(n\text{-}BuOH)^+$ becomes constant as reaction 10 approaches equilibrium. At longer reaction times,

$$Mg(i\text{-}PrOH)^+ + n\text{-}BuOH \underset{k_r}{\overset{k_f}{\rightleftharpoons}} Mg(n\text{-}BuOH)^+ + i\text{-}PrOH \qquad (10)$$

the abundance of secondary product ions increases appreciably, indicating that $Mg(i\text{-}PrOH)^+$ and $Mg(n\text{-}BuOH)^+$ are no longer at their equilibrium concentrations. Figure 4 shows the relative variation of only $Mg(n\text{-}BuOH)^+$ and $Mg(i\text{-}PrOH)^+$ abundances and of their ratio $Mg(n\text{-}BuOH)^+/Mg(i\text{-}PrOH)^+$ with time in the same experiment as in Figure 3. The behavior described above is more evident here and three steps can be distinguished: (a) initial generation of MgL^+ from the reaction of Mg^+ with *i*-PrOH and *n*-BuOH proceeds at different rates for the two molecules ($\sim$200 ms); (b) as Mg^+ decreases, displacement reaction 10 occurs and approaches equilibrium ($\sim$400 ms); (c) the equilibrium is shifted by secondary condensation reaction 7 ($\sim$600 ms), which occurs at different rates for $Mg(i\text{-}PrOH)^+$ and $Mg(n\text{-}BuOH)^+$. The ratio of ion abundances at equilibrium, together with the measured partial pressures of *i*-PrOH and *n*-BuOH, give an equilibrium constant of $K_{eq} = 1.5$. The average of three determinations, obtained for three different *i*-PrOH/*n*-BuOH partial pressure ratios, is $K_{eq} = 1.7 \pm 0.2$, yielding a free-energy difference $\Delta G_{exchange} = -0.30 \pm 0.08$ kcal/mol, as calculated from the relation $\Delta G = -RT \ln K$ at $T = 298$ K.

(23) Su, T.; Bowers, M. T. *Int. J. Mass Spectrom. Ion Phys.* **1973**, *12*, 347.
(24) Nelson, R. D., Jr.; Lide, D. R., Jr.; Maryott, A. A. *Natl. Stand. Ref. Data Ser. (U.S. Natl. Bur. Stand.)* **1967**, *10*.
(25) Miller, K. J.; Savchick, J. A. *J. Am. Chem. Soc.* **1979**, *101*, 7206.
(26) Uppal, J. S.; Staley, R. H. *J. Am. Chem. Soc.* **1982**, *104*, 1229.
(27) (a) McLuckey, S. A.; Cameron, D.; Cooks, R. G. *J. Am. Chem. Soc.* **1981**, *103*, 1313. (b) McLuckey, S. A.; Schoen, A. E.; Cooks, R. G. *Ibid.* **1982**, *104*, 848.

Table II. Relative and Absolute Gas-Phase Ligand Binding Energies to Mg^+ for Various Organic Molecules[a]

Ligand (L)	Measured $\Delta G_{exchange}$[b]	$D^\circ(Mg^+-L)$ rel.[c]	abs.[d]
MeCOEt		7.64	68
	1.24		
Me_2CO		6.40	67
	1.05 1.20		
THF[e]		5.41	66
	0.23		
Et_2O		5.16	66
	0.52 1.61		
n-PrCHO		4.60	66
	0.86 1.45		
n-BuOH		3.87	65
	1.76 0.30		
EtCHO		3.67	65
	0.72 0.93		
i-PrOH		3.59	65
n-PrOH		2.95	64
	0.68 1.17		
MeCHO		2.28	63
	0.52		
EtOH		1.77	63
	1.77		
MeOH		0.00	61

[a] All data are in kcal/mol. [b] For the equilibrium reaction 3 in text. [c] Values (±0.1 kcal/mol) are relative to $D^\circ(Mg^+-MeOH)$ = 0.00 kcal/mol. [d] Absolute values (±5 kcal/mol) assigned from photodissociation results; see text. [e] Tetrahydrofuran.

Equilibria for reaction 3 were measured for various pairwise combinations of organic molecules. $\Delta G_{exchange}$ values from these experiments are reported in Table II. Each value is obtained by averaging the $\Delta G_{exchange}$ of at least three trials performed at different L/L′ partial pressure ratios. Data are combined into a ladder diagram to give a scale of relative free energies, $\Delta G_{exchange}$, for ligand binding. Redundant determinations in the scale provide a check on the results. Agreement between various pairs is generally better than 0.2 kcal/mol, and the precision of each measurement is ±0.1 kcal/mol.

The second method used to calculate the equilibrium constants was the determination of k_f/k_r for reaction 3. The FTMS sequence has already been described in the Experimental Section. Under the conditions in which the forward reaction was studied, no reverse reaction could take place because L′ was the only neutral present in the FTMS cell at this step of the experiment. The small amount of L, which is released by the reactant ion MgL^+, is negligible and is continuously pumped away. Competitive addition reactions of L′ to MgL^+ to give $MgLL'^+$ did not interfere with the substitution rate constant calculation. The partial pressure of the neutral reactant L′ was kept low ($\sim 1.0 \times 10^{-7}$ torr) in order to avoid formation of the $Mg(L')_2^+$ complex. A trapping delay of 1 s preceding isolation of MgL^+ permits its thermalization to occur both by IR radiative decay and by allowing about 10 collisions with the neutral reactant L′.

Figure 5 shows the variation of ion abundance with time for the determination of k_r in reaction 10. The decay of the reactant ion $Mg(n\text{-BuOH})^+$ is described by pseudo-first-order reaction kinetics, eq 11 and 12, where n is the number density of i-PrOH.

$$-d[Mg(n\text{-BuOH})^+]/dt = k_r[Mg(n\text{-BuOH})^+][i\text{-PrOH}] \quad (11)$$

$$\ln [Mg(n\text{-BuOH})^+]_0/[Mg(n\text{-BuOH})^+] = nk_rt \quad (12)$$

In Figure 6 the natural logarithm of the ratio $[Mg(n\text{-BuOH})^+]_0/[Mg(n\text{-BuOH})^+]$ is plotted versus time. The linearity

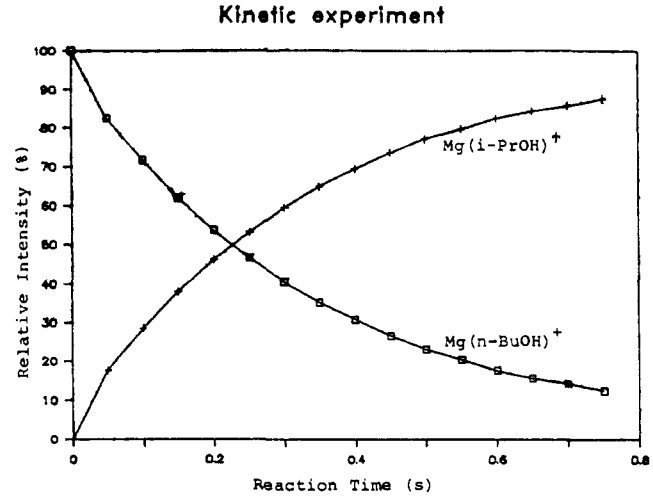

Figure 5. Variation of $Mg(i\text{-PrOH})^+$ and $Mg(n\text{-BuOH})^+$ abundances with time. $Mg(n\text{-BuOH})^+$ has been previously isolated and reacts with i-PrOH after n-BuOH has been pumped away.

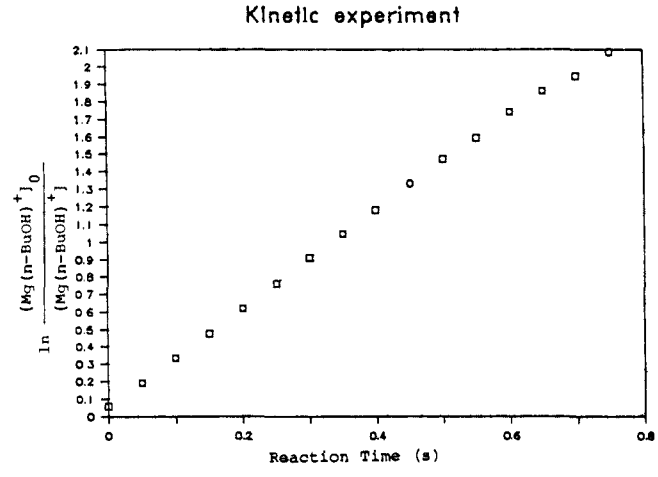

Figure 6. Variation of the natural logarithm of the ratio $[Mg(n\text{-BuOH})^+]_0/[Mg(n\text{-BuOH})^+]$ with time. Data taken from Figure 5.

of these results is consistent with thermalization of the reactant ions. From the slope of the line and the measured partial pressure of i-PrOH, a value of $k_r = 6.2 \times 10^{-10}$ cm^3 molecule^{-1} s^{-1} is obtained. The analogous experiment is performed for the forward reaction in eq 10 by isolation of $Mg(i\text{-PrOH})^+$ and observation of its decay. The absolute rate constant is calculated to be $k_f = 1.0 \times 10^{-9}$ cm^3 molecule^{-1} s^{-1}. The ratio of the forward and reverse rate constants gives the equilibrium constant $K_{eq} = 1.6$ and the free-energy difference $\Delta G_{exchange} = -0.28$ kcal/mol.

Table III presents the values of forward, k_f, and reverse, k_r, absolute rate constants of the same pairwise organic ligands as in Table II. The k_f/k_r ratios and the equilibrium constants are also compared for the two different methods.

Relative free-energies calculated from these values generally agree within 10%. The largest differences are observed when $\Delta G_{exchange}$ approaches the value of 2.0 kcal/mol. This value was, in fact, a limit on the feasibility of performing the kinetic experiments; beyond this energy difference, the reverse reaction was too slow to give good linearity.

It has been shown that for many transition metal ion–ligand complexes, ML^+, photodissociation thresholds can yield absolute bond energies, $D^\circ(M^+-L)$.[10] This is due to the high density of low-lying electronic states near the thermodynamic threshold or, more simply, these metal containing ions absorb over a broad wavelength region. For Mg^+, it has been shown that photodissociation of $MgOH^+$ to give $D^\circ(Mg^+-OH)$ agrees very well with other techniques.[12] This suggests that many of the MgL^+ species may absorb broadly and that the photoappearance onsets may reflect thermodynamic thresholds. However, these values must

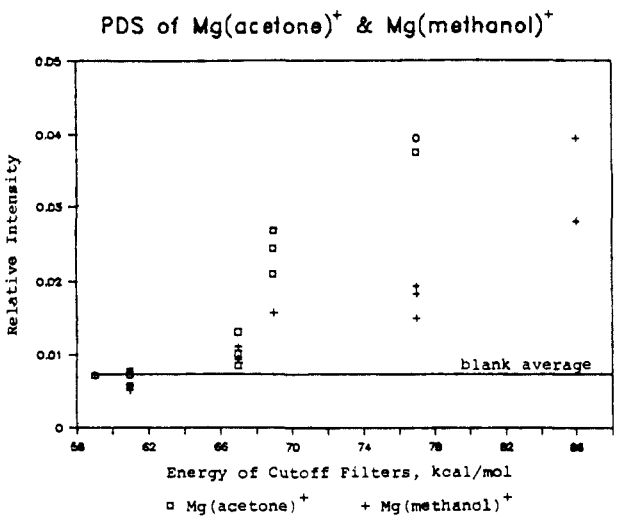

Figure 7. Variation of Mg^+ ion abundance from photodissociation of $Mg(Me_2CO)^+$ (□) and $Mg(MeOH)^+$ (+) with energy of cutoff filters. The solid line is an average of blanks (standard deviation = 0.0010).

Table III. Forward and Reverse Rate Constants for the Equilibrium

$$MgL^+ + L' \underset{k_r}{\overset{k_f}{\rightleftharpoons}} MgL'^+ + L^a$$

L	L′	k_f	k_r	k_f/k_r	k_{eq}[b]
MeOH	EtOH	1.3×10^{-9}	8.7×10^{-11}	15	22
EtOH	MeCHO	1.2×10^{-9}	5.2×10^{-10}	2.3	2.4
EtOH	*n*-PrOH	2.3×10^{-9}	3.1×10^{-10}	7.4	7.1
MeCHO	*n*-PrOH	9.7×10^{-10}	3.7×10^{-10}	2.6	3.2
n-PrOH	EtCHO	8.5×10^{-10}	3.2×10^{-10}	2.7	3.4
n-PrOH	*n*-BuOH	1.3×10^{-9}	2.7×10^{-10}	4.8	4.8
n-PrOH	*n*-PrCHO	5.1×10^{-9}	1.9×10^{-10}	27	20
i-PrOH	*n*-BuOH	1.0×10^{-9}	6.2×10^{-10}	1.6	1.7
i-PrOH	Et_2O	1.5×10^{-9}	1.0×10^{-10}	15	12
EtCHO	*n*-PrCHO	1.7×10^{-9}	5.4×10^{-10}	3.1	4.4
n-BuOH	THF[c]	7.7×10^{-10}	6.6×10^{-11}	12	15
n-PrCHO	Et_2O	7.6×10^{-10}	4.1×10^{-10}	1.8	2.5
Et_2O	THF[c]	9.6×10^{-10}	8.1×10^{-10}	1.2	1.4
Et_2O	Me_2CO	1.3×10^{-9}	2.0×10^{-10}	6.5	7.5
THF[c]	Me_2CO	1.4×10^{-9}	2.4×10^{-10}	5.8	5.8
Me_2CO	MeCOEt	1.6×10^{-9}	2.2×10^{-10}	7.3	8.1

[a] Rate constants are expressed in cm^3 $molecule^{-1}$ s^{-1}. [b] From steady-state measurements. [c] Tetrahydrofuran.

still strictly be considered as upper limits.

Figure 7 illustrates the photodissociation results for $Mg(Me_2CO)^+$ and $Mg(MeOH)^+$ using cutoff filters corresponding to the range 59–86 kcal/mol. The only ionic photoproduct for both experiments was Mg^+ with loss of acetone and methanol, respectively. A normalized intensity of Mg^+/MgL^+, where L = acetone or methanol, was utilized to account for the shot-to-shot variation of the laser. Perusal of this figure shows photodissociation for both systems occurring at energies of 67 kcal/mol and above, while dissociation cannot be distinguished from the blank at 61 kcal/mol. The average of the blanks was 0.0073 with a standard deviation of 0.0010. Therefore, from this data, $61 < D°(Mg^+–MeOH)$, $D°(Mg^+–Me_2CO) < 67$ kcal/mol is indicated. Since the equilibrium studies suggest that $D°(Mg^+–Me_2CO)$ is greater than $D°(Mg^+–MeOH)$ by about 6 kcal/mol, we assign $D°(Mg^+–Me_2CO) = 67 \pm 5$ kcal/mol and $D°(Mg^+–MeOH) = 61 \pm 5$ kcal/mol. Similar photodissociation results were obtained for $Mg(EtOH)^+$ and $Mg(i\text{-}PrOH)^+$, which are in the range 61–67 kcal/mol. The onset for $Mg(MeCOEt)^+$, however, was observed between 67 and 69 kcal/mol with no photodissociation observed using the 67 kcal/mol cutoff filter. This latter result is in excellent agreement with the equilibrium studies (Table II) and provides further confidence in these measurements.

Although the primary focus of this paper is the determination of single ligand bond energies to Mg^+, $D°(Mg^+–L)$, one system was studied to determine the relative binding energies of two ligands to Mg^+ ions using a procedure described earlier by Staley and co-workers.[7c] Summing reactions 8 and 9 yields reaction 13,

$$Mg(L)_2^+ + 2L' \rightleftharpoons Mg(L')_2^+ + 2L \qquad (13)$$

the displacement reaction of both ligands from $Mg(L)_2^+$ to give $Mg(L')_2^+$. The equilibrium constants for reactions 8, 9, and 13 can be determined from the steady-state concentrations of $Mg(L)_2^+$, $MgLL'^+$, and $Mg(L')_2^+$ and from the ratio of pressures of L and L′. The results for L = THF and L′ = acetone, again assuming entropy effects are negligible, indicate that the enthalpy of the first exchange, reaction 8, of $Mg(THF)_2^+$ to give $Mg(THF)(Me_2CO)^+$ is $\Delta H = -0.92$ kcal/mol and for the second exchange, reaction 9, is $\Delta H = -0.38$ kcal/mol. This yields an overall two-ligand exchange enthalpy for reaction 13 of $\Delta H = -1.30$ kcal/mol. It is noteworthy that the enthalpy of the exchange reaction of $Mg(THF)_2^+$ to give $Mg(THF)(Me_2CO)^+$, $\Delta H = -0.92$ kcal/mol, is very close to that of $Mg(THF)^+$ forming $Mg(Me_2CO)^+$, $\Delta H = -0.99$ kcal/mol, as reported in Table II. The forward and reverse rate constants for equilibrium reaction 8, $k_f = 1.4 \times 10^{-9}$ and $k_r = 1.4 \times 10^{-10}$ cm^3 $molecule^{-1}$ s^{-1}, are also similar to those for equilibrium reaction 3, $k_f = 1.4 \times 10^{-9}$ and $k_r = 2.4 \times 10^{-10}$ cm^3 $molecule^{-1}$ s^{-1}. The smaller relative bond energy of the second ligand to Mg^+ suggests a synergistic effect not well understood at this time.

Discussion

Relative and absolute enthalpies of ligand dissociation, reaction 1, for the organic molecules examined are given in Table II. The zero of the relative scale is arbitrarily chosen for $D°(Mg^+–MeOH) = 0.00$ kcal/mol, as it is the weakest bond measured in this study. The relative enthalpy values are obtained directly from the respective free-energy differences with no correction for entropy contributions. The absolute enthalpies have been assigned from both the photodissociation results and the relative enthalpy results. Using $D°(Mg^+–MeOH) = 61 \pm 5$ kcal/mol and $D°(Mg^+–Me_2CO) = 67 \pm 5$ kcal/mol, which are the extremes from the photodissociation results and correlate to the relative enthalpy results as described above, absolute enthalpies have been assigned to the remainder of the MgL^+ species.

Woodin and Beauchamp[28] have discussed in detail entropy changes in the formation of Li^+ complexes by reactions analogous to (4). Starting with the equation:

$$\Delta S = \Delta S_{tr} + \Delta S_v + \Delta S_r + \Delta S_e \qquad (14)$$

where $\Delta S_{tr} = \Delta S$ translational, $\Delta S_v = \Delta S$ vibrational, $\Delta S_r = \Delta S$ rotational, and $\Delta S_e = \Delta S$ electronic, all of the assumptions made for Li^+ can also be applied to Mg^+. First, ΔS_v is a function of the new vibrational modes of the complex, and it is assumed that it only depends on the new Mg^+–L bond. Because of the similarity of these bonds, ΔS_v changes only slightly for different ligands. Second, since ΔS_e is a function of the degeneracy of the ground electronic state of the free ligand and of the Mg^+ complex, the first is assumed to be in its closed-shell ground electronic state. This assumption means ΔS_e depends only on the Mg^+ ground electronic state which undoubtedly is the same for all of the complexes. ΔS_{tr} can be easily determined for all of the MgL^+ complexes because it is a function of the absolute temperature and of the mass of the metal cation Mg^+, the free ligand L, and the complex MgL^+. The translational entropies of the smallest (MeOH) and of the largest (*n*-BuOH and Et_2O) molecules studied are calculated to be $\Delta S_{tr} = -33.8$ and -34.6 eu, respectively. The difference, 0.8 eu = 0.24 kcal/mol at 298 K, even if small, is not always negligible. The rotational entropy, ΔS_r, depends on the rotational symmetry numbers and on the moments of inertia of the complex MgL^+ and of the organic molecule L. Assuming that the geometry of the complexes examined is the same as the corresponding free ligands with Mg^+ placed at the appropriate distance, there would be no variation in rotational symmetry. To the contrary, however, it has been evidenced that moments of inertia can change significantly and strongly effect ΔS_r.[28]

(28) Woodin, R. L.; Beauchamp, J. L. *J. Am. Chem. Soc.* **1978**, *100*, 501.

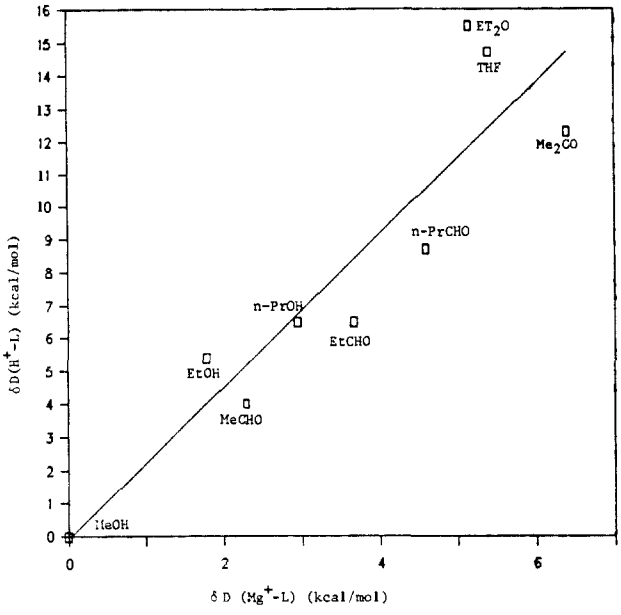

Figure 8. Comparison of relative binding energies of molecules to H^+ and Mg^+. The solid line is a least-squares fit to the data.

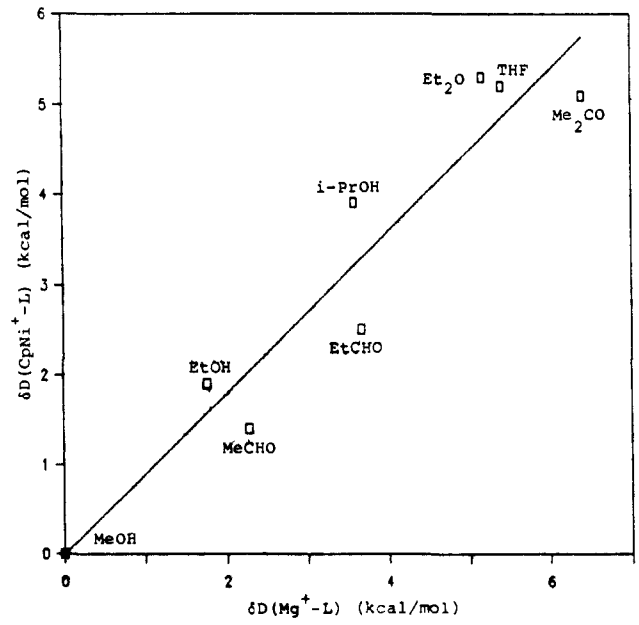

Figure 9. Comparison of relative binding energies of molecules to $CpNi^+$ and Mg^+. The solid line is a least-squares fit to the data.

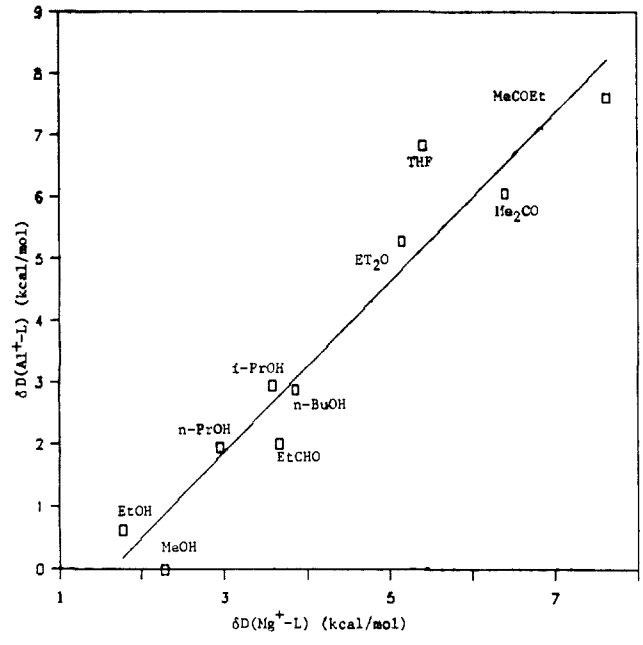

Figure 10. Comparison of relative binding energies of molecules to Al^+ and Mg^+. The solid line is a least-squares fit to the data.

Therefore, variations of entropy ΔS, as expressed in eq 14, are mainly due to changes in the mass of the ligands and to changes in moments of inertia. Unfortunately, at present accurate calculation of the latter contribution is not possible for MgL^+ complexes because their geometries are not available.

The validity of the assumption that entropy changes can be neglected depends on the value of the free-energy difference. When it is small, $|\Delta G_{exchange}| < 0.30$ kcal/mol, it becomes comparable to the entropy changes, which may explain the inversion of some of the relative ligand bond strengths observed in a comparison of CID results and equilibrium constant determinations. Within a series of ligands of the same functional type, CID of $MgLL'^+$ complexes can provide a direct evaluation of the relative bond strength of the two ligands to Mg^+,[27] while the equilibrium constants for ligand exchange reaction 3 are correlated to the free-energy difference. The results obtained by these two methods generally agree except for *n*-BuOH with respect to EtCHO and *i*-PrOH. CID of the complex ions Mg(*i*-PrOH)(EtCHO)$^+$, Mg(EtCHO)(*n*-BuOH)$^+$, and Mg(*i*-PrOH)(*n*-BuOH)$^+$ suggests that $D°(Mg^+–EtCHO) \geq D°(Mg^+–i\text{-PrOH}) \geq D°(Mg^+–n\text{-BuOH})$. For the three pairwise combinations of ligands, however, the difference of fragment ion abundances is very small, suggesting that their bond energies to Mg^+ are very similar. Contrary to the ordering indicated by CID, equilibrium experiments indicate that *n*-BuOH displaces both EtCHO and *i*-PrOH with $\Delta G_{exchange} = -0.20$ and -0.28 kcal/mol, respectively.

Within each class of compounds, alkyl substitution is seen to have a systematic effect: alcohol bond energies increase in basicity in the sequence Me < Et < *n*-Pr < *i*-Pr < *n*-Bu. Similar behavior has been observed for proton affinity, $D°(H^+–L)$,[13] and binding energies to various metal cations,[7,14] and in general can be attributed to the increase in polarizability with the size of the substituent affording greater "internal solvation".

Mg^+ has a $[Ne](3s)^1$ electronic configuration. The charge on Mg^+ attracts ligands by interaction with intrinsic or induced ligand dipoles. For n-donor bases, some covalent bonding occurs by delocalization of electrons from occupied ligand orbitals into the empty 3p or half-filled 3s orbital of Mg^+. Repulsion by the $(3s)^1$ electron should limit this delocalization. $Mg^+–L$ bonding is, therefore, expected to have mainly an ionic character.

Comparison of the ligand dissociation enthalpies for Mg^+ with available results for other reference acids yields interesting information on the nature of the metal ligand interaction. Figure 8 shows the comparison of relative binding energies of organic molecules to H^+[13] and Mg^+. A least-squares fit for alcohols, aldehydes, and ketones gives $\delta D(H^+–L) = 2.31\delta D(Mg^+–L) - 0.10$ kcal/mol (correlation coefficient, $r = 0.84$). This is a reasonable correlation considering that bonding to the proton is much stronger and has a greater covalent character than Mg^+. The slope of this line, 2.31, shows that at increasing ligand basicity, the strength of the bond to H^+ increases faster than that to Mg^+. This supports the expectation that the charge center in the MgL^+ complex is further from the center of the ligand than in HL^+.

Comparison of relative binding energies to $CpNi^+$[14] and Mg^+ is shown in Figure 9. The data show a good linear correlation. A least-squares fit is given by $\delta D(CpNi^+–L) = 0.90\delta D(Mg^+–L) - 0.02$ kcal/mol (correlation coefficient, $r = 0.91$). The slope of this line, 0.90, shows that the substituents have a greater effect on the basicity with respect to Mg^+ than with respect to $CpNi^+$. It is likely that this smaller substituent effect is due to the presence of a second ligand on the $CpNiL^+$ species which, once again, results in the charge center being further away from the ligand.

The comparison of $\delta D(Al^+–L)$[7a] with $\delta D(Mg^+–L)$ is shown in Figure 10. A least-squares fit to the data gives $\delta D(Al^+–L) = 1.37\delta D(Mg^+–L) - 2.24$ kcal/mol with a correlation coefficient of 0.92. The correlation is very good as one might expect, since

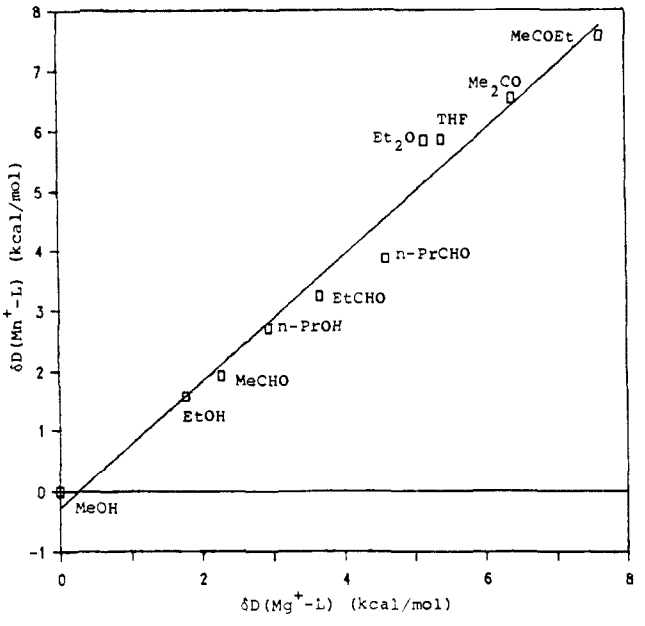

Figure 11. Comparison of relative binding energies of molecules to Mn^+ and Mg^+. The solid line is a least-squares fit to the data.

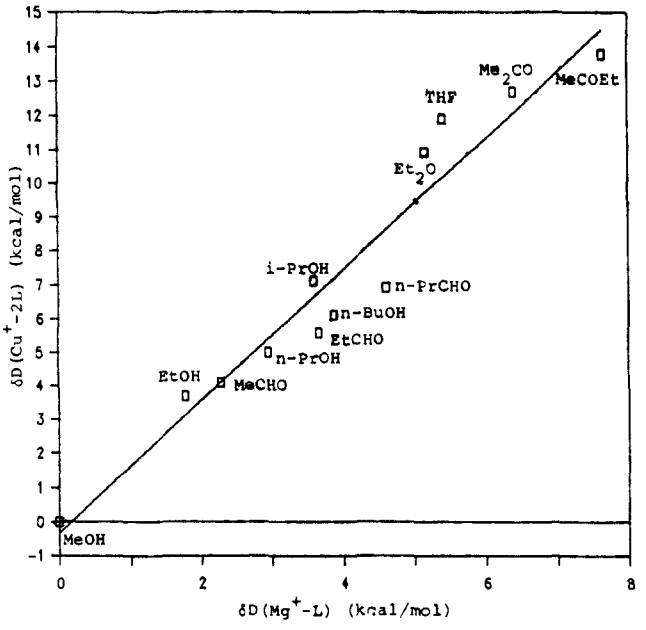

Figure 12. Comparison of relative binding energies of molecules to Cu^+ and Mg^+. The solid line is a least-squares fit to the data.

the bonding to Al^+ and Mg^+, which both lack d electrons, should be similar and have a strong ionic character. The slope of the line, 1.37, indicates a stronger substituent effect for Al^+ than Mg^+. It also suggests that the metal–ligand bond length is shorter for AlL^+ complexes than for MgL^+ complexes.

A comparison of ligand binding energies to Mn^+[7b] and Mg^+ is shown in Figure 11. A least-squares fit to the data gives $\delta D(Mn^+–L) = 1.05\delta D(Mg^+) - 0.28$ kcal/mol (correlation coefficient, $r = 0.97$). The slope of the line, 1.05, is very close to 1.00 and indicates that the nature of the interaction of Mn^+ with these molecules is very similar to that for Mg^+. Also, Mn^+ has a configuration, $[Ar](3d)^5(4s)^1$, with a half-filled s orbital, and it is likely that the d electrons are not involved in bonding to oxygen bases.

Figure 12 shows a plot of relative ligand binding energies to Cu^+,[7c] $\delta D(Cu^+–2L)$, vs. Mg^+, $\delta D(Mg^+–L)$. A least-squares fit of these data is given by $\delta D(Cu^+–2L) = 1.94\delta D(Mg^+–L) - 0.33$ kcal/mol with a correlation coefficient of 0.94. Dividing the slope by 2 to give the relative dissociation enthalpy for each ligand to Cu^+, the slope becomes 0.97. The bonding interaction of Cu^+ with organic molecules is also likely to be similar to that of Mg^+. The electronic configuration of Cu^+ is $[Ar](3d)^{10}$ and covalent bonding can occur only by delocalization of electrons into 4s and 4p orbitals, as the 3d orbitals are already filled.

The zero in each of these comparison plots is arbitrarily assigned to the molecule forming the weakest metal ion–ligand bond. Therefore, the intercepts have no meaning. The slopes of the comparison plots of Mg^+ with the other reference acids vary in the order H^+ (2.31), Al^+ (1.37), Mn^+ (1.05), Cu^+ (0.97), and $CpNi^+$ (0.90). The same order has been observed for correlation plots of these cations with one another.[7b] This order is also likely to reflect the relative metal–ligand bond length. Therefore, the ligand bond distance of Mg^+ is probably longer than that of H^+, and Al^+, similar to that of Mn^+ and Cu^+, and shorter than that of $CpNi^+$. Finally, it has been previously reported[7b] that molecules for each functional group are expected to fall on different lines and that some of these lines may happen to be approximately the same. This is also the general finding of this study.

Conclusion

Four independent methods for determining metal–ligand binding energies have been demonstrated using FTMS: collision-induced dissociation, photodissociation, and the determination of equilibrium constants by both steady-state and kinetic methods. From the combined results, relative and absolute binding energies for 12 ligands to Mg^+ have been assigned. The relative binding energies of Mg^+ were compared with H^+, $CpNi^+$, Al^+, Mn^+, and Cu^+ which yielded, in general, good correlation and provided insight as to the nature of the Mg^+–ligand interaction.

Acknowledgement is made to the Division of Chemical Sciences in the Office of Basic Energy Sciences in the U.S. Department of Energy (DE-FG02-87ER13766) for supporting this research and to the National Science Foundation (CHE-8612234) for providing funds to the advancement of FTMS methodology. L.O. thanks Consiglio Nazionale delle Ricerche (Italia), and E.C.T. thanks Lawrence Livermore National Laboratory for providing fellowship support. Finally, the authors wish to thank co-workers Tim MacMahon and Leo M. Lech for help during the revision stage of this manuscript.

Registry No. THF, 109-99-9; $Mg(MeOH)^+$, 113353-81-4; $Mg(EtOH)^+$, 113353-82-5; $Mg(MeCHO)^+$, 113353-83-6; $Mg(n\text{-}PrOH)^+$, 113353-84-7; $Mg(EtCHO)^+$, 113353-85-8; $Mg(n\text{-}BuOH)^+$, 113353-86-9; $Mg(n\text{-}PrCHO)^+$, 113353-87-0; $Mg(Et_2O)^+$, 113353-88-1; $MgTHF^+$, 113353-89-2; $Mg(Me_2CO)^+$, 113353-90-5; $Mg(MeCOEt)^+$, 113353-91-6; $CpNi^+$, 52668-78-7; Al^+, 14903-36-7; Mn^+, 14127-69-6; Cu^+, 17493-86-6; H^+, 12408-02-5; EtOH, 64-17-5; MeCHO, 75-07-0; *n*-PrOH, 71-23-8; *n*-BuOH, 71-36-3; *n*-PrCHO, 123-72-8; Et_2O, 60-29-7; EtCHO, 123-38-6; Me_2CO, 67-64-1; MeCOEt, 78-93-3.